Investigation of effective line intensities of trans-HONO near 1255 cm^{-1} using continuous-wave quantum cascade laser spectrometers

Xiaojuan Cui [a,b], Fengzhong Dong [b], Markus W. Sigrist [c], Zhirong Zhang [b], Bian Wu [b], Hua Xia [b], Tao Pang [b], Pengshuai Sun [b], Eric Fertein [a], Weidong Chen [a,*]

[a] Laboratoire de Physicochimie de l'Atmosphère, Université du Littoral Côte d'Opale, 189A, Av. Maurice Schumann, 59140 Dunkerque, France
[b] Anhui Institute of Optics & Fine Mechanics, Chinese Academy of Sciences, 230031 Hefei, China
[c] ETH Zurich, Institute for Quantum Electronics, Otto-Stern-Weg 1, CH-8093 Zurich, Switzerland

ARTICLE INFO

ABSTRACT

Effective line intensities of P branch transitions of trans-nitrous acid (HONO) in the ν_3 H-O-N bending mode near 1255 cm^{-1} have been determined by scaling measured HONO absorption intensities by continuous-wave quantum cascade laser absorption spectroscopy to reference values. Gaseous HONO samples were synthetized in the laboratory using the reaction of H_2SO_4 and $NaNO_2$ solutions and the heterogeneous formation on surfaces in the presence of ambient water vapor and NO_2 gas in a sealed gas sampling bag. The quantification of HONO was performed using a denuder associated with a NO_x analyzer. Observed absorption line strengths for the trans conformer are found to be by a factor of approximately 1.17 higher than previously reported line strengths.

1. Introduction

The photolysis of nitrous acid (HONO) is an important source of hydroxyl (OH) free radicals in the atmosphere. Recent field studies indicate a very high contribution of HONO to OH radicals, up to 80% of the integrated source strength [1,2]. The hydroxyl radical is one of the main drivers of atmospheric hydrocarbons oxidation and a key species in the photochemical cycles responsible for tropospheric ozone formation which leads to the so called "photochemical smog" in polluted regions [3]. HONO plays thus an important role in the atmospheric oxidation capacity that significantly affects the regional air quality and global climate change [4]. The comprehensive understanding of the important roles of HONO in the key chemical processes of radicals and the formation of photochemical ozone requires accurate measurements of the HONO concentration. Field observations show that modeled HONO concentrations are often significantly lower than observed values, suggesting a large missing source of HONO [5–7]. This is due to the difficulty in measuring this chemically reactive short-lived species. HONO is also an important indoor air pollutant, it irritates our lungs and eyes [8,9]. Reactions with secondary and tertiary amines can lead to cancerogenic nitrosamines under atmospheric conditions, the effect of which has been commonly called "third-hand" smoke [10–12].

There are various techniques used for atmospheric HONO monitoring. They can be divided into two categories: (1) Analysis of HONO in the aqueous phase after chemical conversion by wet chemical extraction. It is based on the derivatization of gaseous HONO which is captured in liquid form and then quantified by chromatography, photometry, or chemiluminescence [13–15]. Though these methods can offer near part-per-trillion (ppt) levels sensitivity, they are potentially prone to chemical interference, the need for long-time extraction and integration times of usually up to a few minutes. This leads to a large sample residence time [16,17]. (2) Detection of HONO in the gas phase using absorption spectroscopy. Methods such as differential optical absorption spectroscopy (DOAS), incoherent broadband cavity enhanced absorption spectroscopy (IBBCEAS) and the long-path absorption photometer (LOPAP), can get several hundred ppt-level detection limits, but the integration time is long, usually up to several minutes [16,18–20]. The main disadvantage of the DOAS system is that its spatial resolution is rather poor with a path length generally greater than 1 km. For IBBCEAS, the mirrors need to be cleaned regularly, affecting the continuous measurements of atmospheric species. In the mid-infrared region, tunable laser absorption spectroscopy (TLAS) involving continuous-wave quantum cascade lasers (cw-QCL) combined with a multipass absorption cell was applied to the measurement of atmospheric HONO with a sub-ppb detection limit [21–24]. The advantages of using cw-QCLs over lead salt lasers are better mode stability, higher laser output power and room temperature operation without the need for cryogenic cooling, which facilitates long-term field measurements. Particularly, the broadly tunable external cavity QCL (EC-QCL) enables detection of multiple atmosperic species and also detection of larger molecules with broad infrared absorption features [25,26].

The effective line strengths as a function of frequency are necessary parameters for the spectroscopic determination of the HONO concentration. However, only few data on the fundamental rotational-vibrational transitions of HONO in the mid-infrared spectral region have been published and show some inconsistencies [21,27–30]. In this paper, we re-determined four HONO effective absorption line intensities between 1254.6 and 1255.05 cm^{-1} which were also listed in Ref. [21] with a distributed feed-back quantum cascade laser (DFB-QCL) and direct absorption spectra. Furthermore, we determined the line strengths of the other new trans-HONO absorption lines of the ν_3 band in the range of 1251.8–1257.2 cm^{-1} with an EC-QCL on the basis of the re-calibrated line intensity at 1254.8486 cm^{-1} as scaling reference.

We report on the *effective* line strengths of trans-HONO near 1255 cm^{-1}, i.e. the absorbance of light by trans-HONO per unit column density of total (cis and trans) HONO. Hence, the effective line strengths refer to an equilibrium mixture between cis- and trans-HONO at the measurement temperature. The determination of *absolute* line strengths, i.e. absorbance per unit column density of solely trans-HONO, would be less accurate as the cis-trans equilibrium constant exhibits a rather large uncertainty [27,31,32]. During our measurements, the gas samples are always maintained at a constant temperature of 293 K to
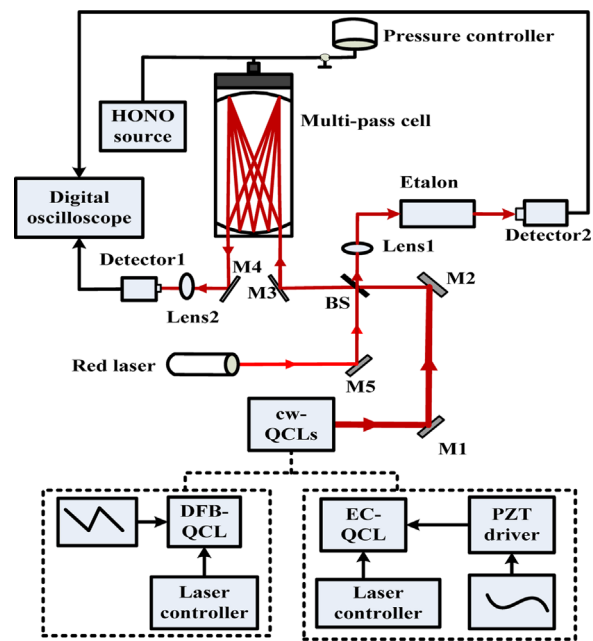

Fig. 1. Schematic diagram of the experimental setup. M: mirror; BS: beam splitter.

avoid any error caused by temperature variations and ensure accurate total HONO quantification. We compare our results to previous line strengths reported by Becker et al. [21] (hereafter referred to as KHB) and discuss optimal spectral regions in which to measure ambient HONO.

2. Experimental details

2.1. Instrument specifications

The two cw- QCL spectrometers involved in the present work are depicted in Fig. 1. The system for gas generation and quantification is described in the following sections. The first cw-QCL we used in 2011 to re-determine effective absorption line intensities of four HONO transitions between 1254.6 and 1255.05 cm^{-1} was a DFB-QCL (DQ7-M776H, Maxion Technologies, Inc.) that emitted single mode with an output power of up to 35 mW and 2 cm^{-1} tuning range. The wavelength range of interest was scanned by ramping the diode injection voltage or changing the temperature. The second cw-QCL employed in the present study is an EC-QCL (41078-MHF, Daylight Solutions). It has a wider tuning range (single mode) of $\sim$40 cm^{-1} from 1223 cm^{-1} to 1263 cm^{-1} and a higher output power of up to 87 mW. A 50 Hz sinusoidal waveform with 3.2 V amplitude and 1.7 V offset from a function generator was first amplified (30 times) using a piezo-electric transducer (PZT) driver (3-Axis Piezo Controller Model MDT690, Thorlabs). The amplified signal of about 100 V was then applied to the PZT element of the EC-QCL to modulate the external cavity grating to scan the EC-QCL frequency over $\sim$5 cm^{-1} across the absorption lines of HONO which are measured in this article. The frequency tuning of the EC-QCL is performed sinusoidally only.

Sinusoidal instead of sawtooth or triangular modulation is preferred because rapid changes in the scan direction resulting from the use of a sawtooth or triangular ramp signal will cause excitation of mechanical vibrations, rendering the laser output unstable and resulting in permanent laser damage. The instrumental half widths at half-maximum for the two QCLs are less than $0.0005 \, cm^{-1}$. This was determined by scanning nearby CH_4 absorption lines at $1255 \, cm^{-1}$, for which absorption line parameters are readily available from databases or references, at gas pressures below 5 Torr to minimize collisional broadening. The pressure-dependent line width of HONO absorption lines was measured in synthetic air at different cell pressures from 8.5 to 40 Torr. A γ_{air} value of $0.0012 \pm 0.0002 \, cm^{-1} \, Torr^{-1}$ was obtained for the trans conformer of HONO near $1255 \, cm^{-1}$.

The laser beams of the two QCLs first pass through a beamsplitter and are split into two separate components (90% transmission and 10% reflection). The transmitted light is directed into a multi-pass cell (Model 107-V, Infrared Analysis, Inc.) with a 152 m folded path length in a volume of 16 L. A red laser beam is injected into the system via a mirror and co-aligned with the mid-infrared beam to facilitate beam alignment with the multi-pass cell. The emerging absorption signal from the multi-pass cell is focused onto detector 1 (PVI-4TE-10.6, Vigo detector) by means of a lens with a focal length of 5 cm. The reflected light is directed into a Fabry-Perot etalon with a free spectral range of $\sim 0.04 \, cm^{-1}$, measured by detector 2 (PVMI-10.6, Vigo detector) for wavelength calibration. The total pressure in the multi-pass cell is measured and controlled by a pressure gauge (Pfeiffer Vacuum). The absorption signal is acquired with a 5 Gsample/s, 1 GHz bandwidth digital oscilloscope (104Xs-A, LeCroy Wavesurfer).

2.2. HONO sample synthetization

Two methods are used to generate HONO in this work. The first one is the liquid phase method we used in 2011. Gas-phase samples of nitrous acid are prepared according to a method previously described in Ref. [33,34]. A dilute 0.1% $NaNO_2$ solution contained in a dropping funnel is added slowly to a dilute 0.5% H_2SO_4 solution in a 3-neck flask through one neck of the flask. The chemical reaction is listed as reaction (R1) below. The flask is cooled by the ice water mixture to reduce the temperature and heat from sulfuric acid. Air or nitrogen is allowed to flow into the vessel through the second neck of the flask and is directed upward by the inlet tube at the solution face. During the synthesis, the gaseous nitrous acid is flushed into a dark bag which is connected to the third neck of the flask using the flow of nitrogen. The HONO synthesis is carried out in the dark to avoid photolysis. The advantage of this method is that all the materials are very easy to be acquired in the laboratory, and the generation procedure is also facile to be operated and controlled. However, this synthesis does not only produce HONO, it also forms NO, NO_2, H_2O and HNO_3 by reactions (R2) and (R3). This is not a problem since the other gases do not have strong absorbance at our laser wavelength range, and the EC-QCL measurement system we use does not detect any interference from other gases except for several weak H_2O absorption lines.

$$NaNO_2 + H_2SO_4 \rightarrow NaHSO_4 + HONO \qquad (R1)$$

$$2HONO \leftrightarrow NO + NO_2 + H_2O \qquad (R2)$$

$$HONO + NO_2 \rightarrow NO + HNO_3 \qquad (R3)$$

The second method employed in this study is the gas phase method. This method is very advantageous, because HONO at ppm levels is produced easily by heterogeneous formation on surfaces in the presence of ambient water vapor and 800 ppm NO_2 gas (see reaction (R4)) in a sealed static gas sampling bag (5 l, SKC Quality sample bag) [35].

$$H_2O + NO_2 \rightarrow HONO + HNO_3 \qquad (R4)$$

This reaction quickly generates gaseous HONO in the presence of a gas sampling bag containing a high concentration of NO_2 gas. However, the quantification of HONO would be difficult to perform, because the mixing ratio of the water vapor on the surfaces is unknown, and
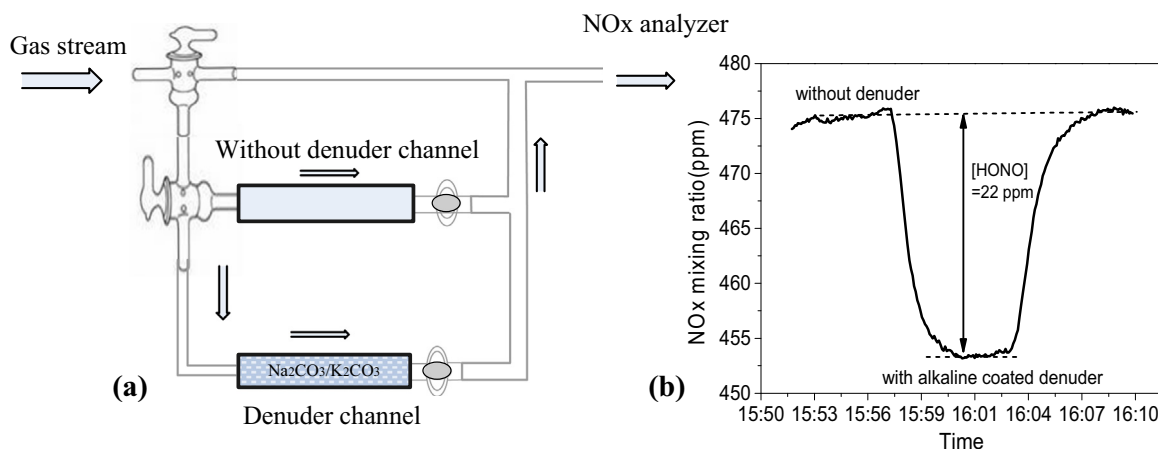

Fig. 2. Schematic of HONO quantification: (a) Setup with denuder and reference channel; (b) NO_x mixing ratio versus time when alternating between the two channels.

the heterogeneous reaction in the bag is always in progress. We will describe in detail why we choose this method without the need to carry out HONO quantification in the following Section 2.4.2.

2.3. Quantification of gaseous HONO

A practical method involving conventionally available technologies for the quantification of the synthesized short-lived reactive species is important for validation and calibration of the newly developed emerging instrumentation. The first denuder configuration proposed for HONO quantification is reported by M. Ferm and I. Allegrini et al. [36,37], and is relied on the use of two sodium carbonate-coated denuders. The mixing ratio of HONO generated by the reaction of H_2SO_4 and $NaNO_2$ solutions (reaction R_1 above) is quantified in 2011 by using the denuder technique associated with a conventional chemiluminescence NO_x analyzer (Hartmann and Braun) [23,38–41]. The gas sample flow from the synthesis system is directed alternately through a channel containing a denuder tube with a length of 30 cm and a diameter of 1.1 cm (filled with alkalic coating: K_2CO_3/Na_2CO_3 to trap acid) and another same-sized channel without denuder, prior to entering the NO_x analyzer to measure HONO and nitrogen oxides such as NO_2, NO etc. produced by reactions R1–R3 (see Fig. 2). The mixing ratio of HONO is calculated based on the difference of the mean values between the two channels. The average is obtained by applying statistical methods to the data of each channel. Nitric acid (HNO_3) generated by reaction R_3 is negligible because it has a much slower response time through the system due to surface interaction than those exhibited by NO and NO_2 [27]. Moreover, we simulated a 5 ppm HNO_3 spectrum (see Fig. 5 which will be described in Section 2.4.2). Even if a high mixing ratio HNO_3 (5 ppm) is simulated, the absorbance of HNO_3 is still too weak to be detected with our QCL system which exhibits a detection limit of absorbance of 0.01, i.e. if the absorbance is < 0.01, it will be submerged in the baseline noise. During all the experiments, the generated HNO_3 quantity should be much less than 5 ppm, and we indeed did not detect any HNO_3 absorption lines. The mixed gas streams (HONO, NO_2, NO etc.) with the flow of air or nitrogen are controlled at a steady gas flow rate of 10 L/h by the flowmeter of the NO_x analyzer to ensure the float in the flowmeter will not fluctuate and to minimize residence times inside the gas tube.

The output gas mixing ratio from the HONO source is increasing (30–60 min) all the time until the value is steady. Once the output gas mixing ratio is stable, the denuder channel will be opened, after the denuder output is constant for 3–5 min, we close the denuder channel. Then the output from the HONO generation system will rise rapidly to the value of stable gas mixing ratio before the denuder. We sample the HONO gas to record spectra before or after the denuder when the once output is stable.

As the denuder method relies on removing acidic species by alkalic components (like Na_2CO_3), the capacity of the denuder and hence the measurement accuracy of HONO mixing ratio truly depend on the alkalic coating and
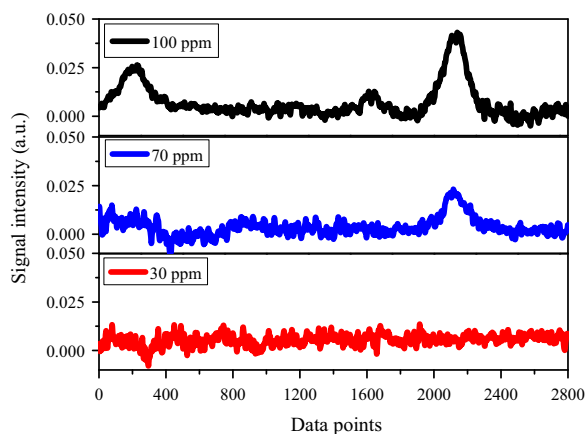

Fig. 3. HONO absorption spectra at different mixing ratios, sampled after the alkalic denuder. The measurements results imply that gaseous HONO samples with mixing ratio < 30 ppmv are totally trapped by the used denuder in the present work.

the HONO mixing ratio to be measured. Correct HONO mixing ratio could be deduced only when the sodium carbonate denuder could trap 100% HONO and without any residual HONO reaching the NO_x analyzer after the denuder filtering.

The efficiency of the denuder used in the present work was carefully checked using absorption spectroscopy measurements. Fig. 3 shows absorption spectra of different mixing ratio gas samples after the denuder. As can be seen, the spectrum of the ~ 70 ppmv HONO sample exhibits still absorption peaks after passing the denuder channel, while the sample of 30 ppmv HONO does not present any absorption features after being filtered by the present denuder system. This result implies that, our denuder system allows the correct determination of HONO mixing ratio below 30 ppmv. The mixing ratio of HONO derived by the denuder technique show good agreement (within 10%) with the spectroscopic measurements over a wide range of mixing ratios (up to 30 ppm).

2.4. Determination of effective line strengths

Based upon the Beer–Lambert law, the absorbance $A(\nu)$ at frequency ν can be expressed as:

$$A(\nu) = \ln\big(I_0(\nu)/I(\nu)\big) = N\sigma(\nu)L \tag{1}$$

where $I(\nu)$ and $I_0(\nu)$ are the transmitted and incident probing light intensity, respectively, N is the number of absorbing molecules (in [molecules/cm^3]), $\sigma(\nu)$ is the frequency-dependent absorption cross section (in [cm^2/molecule]), and L is the optical absorption path length (in [cm]). The integrated absorbance A_I (in [cm^{-1}]) can be written as:

$$A_I = \int A(\nu)d\nu = \int \ln\big(I_0(\nu)/I(\nu)\big)d\nu = NL \int \sigma(\nu)d\nu = NLS \tag{2}$$

The trace mixing ratio of absorbing molecules in the vapor or gas phase is usually expressed in terms of ppmv (parts per million by volume, 10^{-6}), ppbv (parts per billion

by volume, 10^{-9}), pptv (parts per trillion by volume, 10^{-12}) or ppqv (parts per quadrillion by volume, 10^{-15}). Based on Eq. (2), the gas species mixing ratio can be retrieved from the integrated absorbance A_I measured at temperature T and pressure P [42]:

$$C(\text{ppm}) = \frac{N}{N_T} \times 10^6 = \frac{A_I P_0 T}{N_L P T_0 L S} \times 10^6 \qquad (3)$$

The effective line-strength S of trans-HONO can be obtained using Eq. (3).

$$S = \frac{A_I P_0 T \times 10^6}{C N_L P T_0 L} \qquad (4)$$

where $N_L = 2.6868 \times 10^{19}$ mol/cm^3 represents the Loschmidt number at $T_0 = 273.15$ K and $P_0 = 760$ Torr, S is the molecule absorption line strength (in [cm^2/(mol cm)]), C is the HONO mixing ratio in the gas phase (in [ppm]).

2.4.1. Comparison with data from KHB

There are fewer published articles and greater uncertainty in absolute values of the absorption lines for the short-lived specie HONO than the greenhouse gas CH$_4$ where absorption line parameters have been well studied and are readily available in publications or databases such as HITRAN in the mid-infrared spectral region [21,27,28]. We re-determined four HONO absorption line strengths reported by KHB and calculated the new line parameters in the range of 1251.8–1257.2 cm^{-1} using re-determined KHB absorption line intensities (hereafter referred to as RKHB) as scaling reference. Absolute HONO absorption line positions were determined relative to those of nearby methane and/or water vapor absorption lines along with laser frequency tuning rates determined by recorded interference fringes of a Fabry-Perot etalon (see Fig. 1).

We used the calibrated HONO mixing ratio of 22 ppm (as described in Section 2.3) and the DFB-QCL system to re-determine four strong HONO absorption line intensities between 1254.6 and 1255.1 cm^{-1} [21]. The calculated values for the measured ν_3 band of trans-HONO lines are summarized in Table 1 (effective line strengths based on the total HONO concentration of cis and trans isomers, which are in equilibrium at $T = 293$ K).

The main error sources in the determination of four HONO effective line strengths are the HONO mixing ratio (measured by a NO$_x$ analyzer with an accuracy of better than 10%) and the integrated absorbance area A_I (related to pressure-dependent line widths and the laser line width) obtained using non-linear least square fits resulting in an error of about 2%. The errors caused by the determination of the absorbance path length and the gas pressure in the absorption cell are less than 1%.

2.4.2. Determination of new line intensities

The HONO absorption lines across 0.5 cm^{-1} in Fig. 4 were simultaneously recorded at a scan rate of 50 Hz and an integrated time 20 s with the EC-QCL system. The black dotted lines in Fig. 4 are the observed absorbance spectrum during HONO spectra measurement experiments for the trans conformers, while their corresponding non-linear least-square fits are presented in Fig. 4 as red lines. The gas mixing ratio C is thus identical for all

recorded lines in the spectrum according to Eq. (3) with identical gas pressure P, temperature T, and constants P_0, T_0, L and N_L, such that the ratio A_I/S is also equivalent. The new line strengths S_{new} can be expressed as

$$S_{new} = \frac{A_{I(new)} \times S_{1254.8486}}{A_{I(1254.8486)}} \qquad (5)$$

The re-determined line strength at 1254.8486 cm^{-1} (in Table 1) was used to determine the other new HONO absorption line strengths in the range of 1251.8–1257.2 cm^{-1}. The reason for selecting this specific line is that it is free of interferences from other species (CH$_4$, H$_2$O, N$_2$O, NO$_2$, HNO$_3$ etc.), and has less error as scaling reference compare to the other three absorption lines. We simulated absorption spectra of potential interferences species present in the air (2 ppm CH$_4$ and 10% H$_2$O) and the HONO generation sources (400 ppm NO$_2$ and 5 ppm HNO$_3$), as shown in Fig. 5. The first HONO absorption line (marked (1)) will be affected by the nearby HONO line at 1254.72 cm^{-1} and H$_2$O absorption line at 1254.73 cm^{-1}. The third (3) and the fourth (4) absorption lines are adjacent, only the second (2) absorption line is independent from the other three absorption lines. About the errors of four absorption lines, see Table 1, the minimum error ± 0.6 is from the fourth absorption line at 1255.0473 cm^{-1}, but the accuracy of the integrated absorbance area of this absorption line will be influenced by the third absorption line. The second absorption line has less error than the first line, and thus preferably be used as the scaling reference. In contrast to HONO, H$_2$O and CH$_4$, the absorption lines strengths of NO$_2$ and HNO$_3$ are very weak (absorbance of 10^{-23}) and hence undetected during all the experiments.

Accorrding to Eq. (5), the calibration of the HONO mixing ratio is obsolete for the determination of new line strengths using the scaling reference method. This is because we just need to get the integrated absorbance area at the same conditions. As described in Section 2.2, HONO at ppm levels used in this method is produced easily by heterogeneous formation on surfaces in the presence of ambient water vapor and high mixing ratio NO$_2$ gas in a sealed static gas sampling bag.

3. Results and discussion

Absorbance spectra of the ν_3 H-O-N bending mode of the P branch of trans-HONO from 1251.8 to 1257.2 cm^{-1} are shown in Fig. 6. The spectra were recorded at a total pressure of below 8.5 Torr to select individual HONO absorption lines well separated from H$_2$O absorption lines which also appear in this region of the spectrum. Table 2 lists the new absorption line positions and effective line strengths for the HONO trans conformer (the four RKHB absorption lines are also included). We used the pre-determined line intensity value at 1254.8486 cm^{-1} and applied it as a scaling reference to calculate the other new HONO absorption line parameters. Therefore, these additional absorption line intensities do not contribute any quantitative value and should not be used for comparison.

Table 1
Four trans-HONO absorption line positions and effective line strengths deduced in this work (RKHB) and Ref. [21] (by KHB).

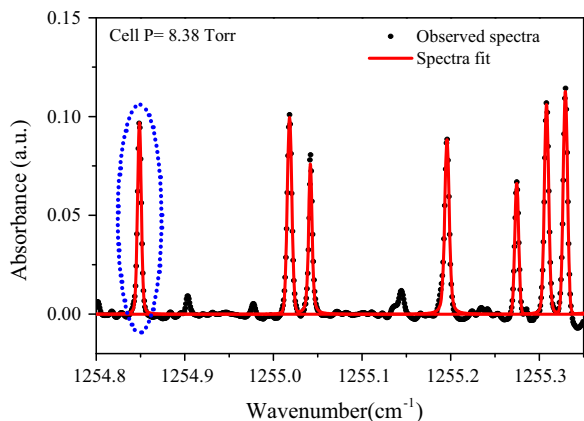| Wavenumber (cm^{-1}) (RKHB)	Effective line strength $(cm^{-1}/(molec\text{-}cm^{-2})*10^{-21})$ (RKHB)	Wavenumber (cm^{-1}) (KHB)	Effective line strength $(cm^{-1}/(molec\text{-}cm^{-2})*10^{-21})$ (KHB)
1254.6832	13.7 ± 1.0	1254.6838	11.8 ± 0.8
1254.8486	11.2 ± 0.8	1254.8489	9.6 ± 0.6
1255.0252	13.1 ± 1.1	1255.0256	11.3 ± 0.9
1255.0473	8.4 ± 0.6	1255.0473	7.2 ± 0.5

Fig. 4. Absorbance spectrum of trans-HONO recorded at a cell pressure of 8.38 Torr with a scan frequency of 50 Hz (Av = 1000) and an optical path length of 152 m. The absorption line marked by the purple oval was used to determine new HONO absorption line strengths. The three small black absorption peaks not fitted are weak HONO absorption lines whose line strengths have not been calculated in this study.
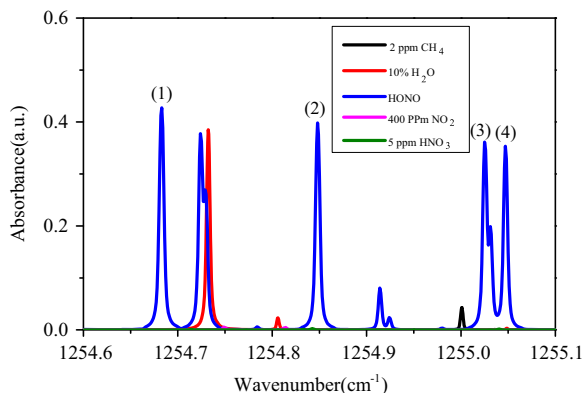

Fig. 5. Recorded HONO spectrum (blue) of unknown mixing ratio generated from the heterogeneous formation and simulated spectrum of 2 ppm CH_4 (black), 10% H_2O (red), 400 ppm NO_2 (violet) and 5 ppm HNO_3 (green) at the same conditions of $L = 152$ m, $P = 8.2$ Torr. The lines marked with numbers are HONO absorption lines listed in Table 1.

We restrict our comparison with KHB data to the four HONO absorption line intensities listed in Table 1.

Fig. 7 compares the four RKHB absorption lines strengths to those of KHB [21]. The absorption line strengths for each of the 4 discernible peaks for the HONO
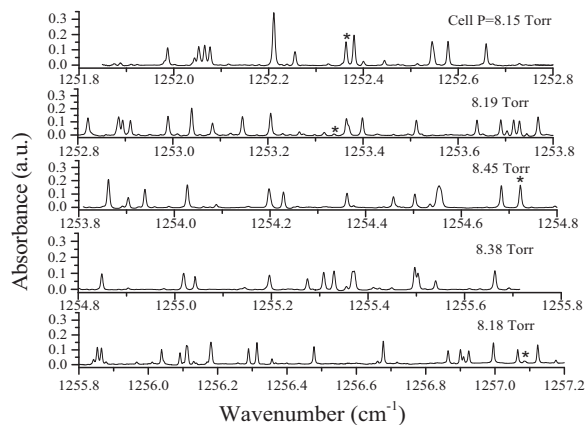

Fig. 6. Measured absorbance spectra of trans-HONO studied in the range of 1251.8–1257.2 cm^{-1} at different cell pressures. The asterisks indicate H_2O absorption lines or H_2O absorption lines which are overlapping with HONO absorption lines.

trans conformer near 1255 cm^{-1} are higher than those of KHB by a factor of approximately 1.17. This discrepancy for the trans-HONO ν_3 band absorption line intensities near 1255 cm^{-1} is most likely the result of the method of generating gaseous HONO and the uncertainty in quantifying HONO. The four RKHB absorption lines are obtained from the reaction of H_2SO_4 and $NaNO_2$ solutions, while KHB produced HONO from a reaction of gaseous HCl with solid $NaNO_2$. KHB extracted gaseous HONO in a basic liquid trap followed by ion chromatography to quantify the nitrite ion and used a chemiluminescence analyzer with molybdenum converter to measure NO and NO_2. In contrast, our study uses the denuder technique associated with a conventional NO_x analyzer to perform the quantification of gaseous HONO. The slightly higher temperature KHB used in his study compared to the 293 K employed in our investigation could only explain a deviation of smaller than 1%. KHB's results are also inconsistent with those of Lee et al. [27], who report effective line strengths of trans-HONO absorption lines near 1275 cm^{-1} and cis- HONO at 1660 cm^{-1}. A key difference between KHB's study and that of Lee et al. is also the way in which gaseous HONO is quantified. In Lee's work, HONO is simultaneously measured by complete conversion followed by continuous NO quantification by calibrated absorption spectroscopy. The uncertainty in the reported line strengths in Lee's study is < 6%, while the error on the reported line strengths is estimated to be < 13% for KHB's data. It should be pointed out that the ratio of the line strengths from the present study and those of KHB for the four HONO absorption lines is almost constant (the standard deviation of all values shown in Fig. 7 is 0.0057) which implies that the relative intensities are identical.

To our knowledge, the effective line strengths data of trans-HONO in the range of 1251.8–1257.2 cm^{-1} in this paper represent the first high resolution mid-infrared line strengths measurements of trans-HONO using TLAS technology after those of the KHB study in 1995, which only discusses 9 lines between 1254.2 and 1255.2 cm^{-1} [21]. A comparison of HONO detection using the TLAS method in the mid-infrared at different wavenumber is summarised

Table 2
Line positions and effective line strengths for the ν_3 band of trans-HONO at 293 K.

Line position (cm^{-1})	Effective line strength (cm^{-1}/(molec-cm^{-2}) *10^{-21})
1251.9867	9.2 ± 0.6
1252.2109	21.1 ± 1.4
1252.2556	7.7 ± 0.5
1252.3635	10.1 ± 0.7
1252.3803	12.8 ± 0.9
1252.5809	11.2 ± 0.8
1252.6591	10.0 ± 0.7
1252.8152	8.9 ± 0.6
1252.9061	7.0 ± 0.5
1252.9901	10.3 ± 0.7
1253.0382	13.3 ± 1.0
1253.0832	7.4 ± 0.5
1253.1525	10.5 ± 0.7
1253.2061	11.9 ± 0.8
1253.4068	10.2 ± 0.7
1253.5126	9.8 ± 0.7
1253.6403	8.5 ± 0.6
1253.6923	9.9 ± 0.7
1253.7172	9.5 ± 0.6
1253.7301	10.1 ± 0.7
1253.7685	10.2 ± 0.7
1253.8621	13.0 ± 0.9
1253.9036	6.6 ± 0.4
1253.9383	10.1 ± 0.7
1254.0281	11.4 ± 0.8
1254.1979	9.3 ± 0.6
1254.2281	9.7 ± 0.6
1254.3607	9.3 ± 0.6
1254.4599	7.9 ± 0.5
1254.5029	9.7 ± 0.6
1254.6832	13.7 ± 1.0
1254.8486	11.2 ± 0.8
1255.0252	13.1 ± 1.1
1255.0473	8.4 ± 0.6
1255.2015	9.5 ± 0.6
1255.2804	7.0 ± 0.5
1255.3147	9.4 ± 0.6
1255.3296	9.5 ± 0.6
1255.5463	4.8 ± 0.3
1255.6647	10.7 ± 0.7
1256.0364	8.3 ± 0.5
1256.0957	4.4 ± 0.3
1256.1818	13.8 ± 0.9
1256.2892	8.9 ± 0.6
1256.3136	10.4 ± 0.7
1256.4775	8.9 ± 0.6
1256.6777	14.3 ± 1.0
1256.8647	7.8 ± 0.5
1256.9242	7.3 ± 0.5
1256.9952	11.8 ± 0.8
1257.0656	8.4 ± 0.6
1257.1233	9.9 ± 0.7

Fig. 7. Effective line strengths from KHB and RKHB, all plotted as a function of wavenumber (cm^{-1}). Listed numbers represent the ratio between line strengths of RKHB to those of KHB with a standard deviation of 0.0057.

Table 3
Comparison of HONO detection using TLAS method in the mid-infrared at different frequency regions.

Wavenumber (cm^{-1}) and reference	Line intensity (cm^{-1}/molecule cm^{-2})	Detection limits (pptv)	Optical path-length (m)
1280.4000 [22]	3.25×10^{-20}	~300 (30 min)	126
1713.5110 [23]	2.59×10^{-20}	~200 (1 s)	153
1660.0000 [24]	1.29×10^{-20}	~300 (1 s)	210
1252.2109 (present work)	2.1×10^{-20}	~400 (1 s)	152

more strongly, the detection sensitivity in our study could be further enhanced by increasing the absorption path length or by reducing the background electronic noise associated with the detector. In addition, the direct absorption method is affected by the low frequency noise of the laser, the detector and the circuit. In combination with high-frequency modulation of the diode laser, sensitivities are expected to be further improved by up to two orders of magnitude compared to direct absorption measurements which have been demonstrated in the Refs. [21,43,44].

4. Conclusion

The ν_3 band of trans-HONO absorption spectrum near 8 μm was studied using cw-QCL spectrometers and HONO mixing ratios was calibrated with a denuder system. The revised four HONO lines strengths are higher by a factor of 1.17 compared to a previous study named KHB [21]. The reasons for this discrepancy are assumed to be both the kind of generating gaseous HONO and the uncertainty in quantifying the mixing ratio. Our approach based on the RKHB absorption line strength at 1254.8486 cm^{-1} as well as a straightforward generation of HONO without need to know its mixing ratio is advantageous for the determination of new effective line strengths with less error. The line at 1252.2109 cm^{-1} with a line intensity of 2.1×10^{-20} cm^{-1}/

in Table 3. The detection limits are given for a signal-to-noise ratio of 1σ and for the listed integration time (30 min or 1 s). Based on our present study, the strongest absorption line of 2.1×10^{-20} cm^2 molecule^{-1} cm^{-1} at 1252.2109 cm^{-1} is very suitable for interference-free monitoring of HONO in ambient air (i.e. no interferences with CO_2, H_2O, CH_4 etc.) at sub-ppb mixing ratios. Our extrapolated detection limit amounts to 400 ppt $(1 s, 1-\sigma)$ which is comparable to the other studies, given the weaker absorbance and shorter optical path length of 152 m. Apart from choosing a spectral region in which HONO absorbs
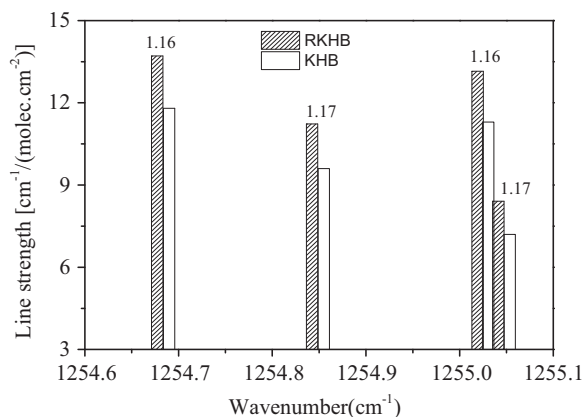
mole cm^{-2} appears very suitable for interference-free monitoring of HONO in ambient air (i.e. no interferences with CO_2, H_2O, CH_4 etc.) at sub-ppb mixing ratios.

Acknowledgments

References

[1] Stemmer K, Ammann M, Donders C, Kleffmannm J, George C. Photosensitized reduction of nitrogen dioxide on humic acid as a source of nitrous acid. Nature 2006;440(7081):195–8.

[2] Li X, Rohrer F, Hofzumahaus A, Brauers T, Häseler R, Bohn B, et al. Missing gas-phase source of HONO inferred from Zeppelin measurements in the troposphere. Science 2014;344(6181):292–6.

[3] Dehayem-Kamadjeu A, Pirali O, Orphal J, Kleiner I, Flaud PM. The far-infrared rotational spectrum of nitrous acid (HONO) and its deuterated species (DONO) studied by high-resolution Fourier-transform spectroscopy. J Mol Spectrosc 2005;234(1):182–9.

[4] Richer A, Burrows JP, Nuß H, Granier C, Niemeier U. Increase in tropospheric nitrogen dioxide over China observed from space. Nature 2005;437(7055):129–32.

[5] Su H, Cheng Y, Oswald R, Behrendt T, Trebs I, Meixner FX, et al. Soil nitrite as a source of atmospheric HONO and OH radicals. Science 2011;333(6039):1616–8.

[6] Heikes BG, Thompson AM. Effects of heterogeneous processes on NO_3, HONO, and HNO_3 chemistry in the troposphere. J Geophys Res 1983;88(C15):10883–95.

[7] Svennson R, Ljungstrom E, Lindqvist O. Kinetics of the reaction between nitrogen dioxide and water vapour. Atmos Environ 1987;21(7):1529–39.

[8] Jarvis DL, Leaderer BP, Chinn S, Burney PG. Indoor nitrous acid and respiratory symptoms and lung function in adults. Thorax 2005;60(6):474–9.

[9] Beckett WS, Russi MB, Haber AD, Rivkin RM, Sullivan JR, Tameroglu Z, et al. Effect of nitrous acid on lung function in asthmatics: a chamber study. Environ Health Perspect 1995;103(4):372–5.

[10] Park SS, Hong JH, Lee JH, Kim YJ, Cho SY, Kim SJ. Investigation of nitrous acid concentration in an indoor environment using an in-situ monitoring system. Atmos Environ 2008;42(27):6586–96.

[11] Zhou XL, Huang G, Civerolo K, Roychowdhury U, Demerjian KL. Summertime observations of HONO, HCHO, and O_3 at the summit of Whiteface Mountain, New York. J Geophys Res Atmos 2007;112(D8). http://dx.doi.org/10.1029/2006JD007256.

[12] Sleiman M, Gundel LA, Pankow JF, Jacob PIII, Singer BC, Destaillats H. Formation of carcinogens indoors by surface-mediated reactions of nicotine with nitrous acid, leading to potential thirdhand smoke hazards. Proc Natl Acad Sci USA 2010;107(15):6576–81.

[13] Dibb JE, Huey LG, Slusher DL, Tanner DJ. Soluble reactive nitrogen oxides at South Pole during ISCAT 2000. Atmos Environ 2004;38(32):5399–409.

[14] Kleffmann J, Heland J, Kurtenbach R, Lorzer J, Wiesen P. A new instrument (LOPAP) for the detection of nitrous acid (HONO). Environ Sci Pollut Res 2002;9(4):48–54.

[15] Zhou XL, Qiao HC, Deng GH, Civerolo K. A method for the measurement of atmospheric HONO based on DNPH derivatization and HPLC analysis. Environ Sci Technol 1999;33(20):3672–9.

[16] Kleffmann J, Lorzer JC, Wiesen P, Kern C, Trick S, Volkamer R, et al. Intercomparison of the DOAS and LOPAP techniques for the detection of nitrous acid (HONO). Atmos Environ 2006;40(20):3640–52.

[17] Liao W, Case AT, Mastromarino J, Tan D, Dibb JE. Observations of HONO by laser-induced fluorescence at the South Pole during ANTCI 2003. Geophys Res Lett 2006;33(L09810). http://dx.doi.org/10.1029/2005GL025470.

[18] Gherman T, Venables DS, Vaughan S, Orphal J, Ruth AA. Incoherent broadband cavity enhanced absorption spectroscopy in the near-ultaviolet: application to HONO and NO_2. Environ Sci Technol 2008;42(3):890–5.

[19] Wu T, Chen W, Fertein E, Cazier F, Dewaele D, Gao X. Development of an open-path incoherent broadband cavity-enhanced spectroscopy based instrument for simultaneous measurement of HONO and NO_2 in ambient air. Appl Phys B 2012;106(2):501–9.

[20] Wu T, Zha Q, Chen W, Xu Z, Wang T, He X. Development and deployment of a cavity enhanced UV-LED spectrometer for measurements of atmospheric HONO and NO_2 in Hong Kong. Atmos Environ 2014;95:544–51.

[21] Becker KH, Kleffmann J, Kurtenbach R, Wiesen P. Line strength measurements of trans-HONO near $1255\ cm^{-1}$ by tunable diode laser spectrometry. Geophys Res Lett 1995;22(18):2485–8.

[22] Schiller CL, Locquiao S, Johnson TJ, Harris GW. Atmospheric measurements of HONO by tunable diode laser absorption spectroscopy. J Atm Chem 2001;40(3):275–93.

[23] Li YQ, Schwab JJ, Demerjian KL. Fast time response measurement of gaseous nitrous acid using a tunable diode laser absorption spectrometer: HONO emission source from vehicle exhausts. Geophys Res Lett 2008;35(L04803). http://dx.doi.org/10.1029/2007GL031218.

[24] Lee BH, Wood EC, Zahniser MS, McManus JB, Nelson DD, Herndon SC, et al. Simultaneous measurements of atmospheric HONO and NO_2 via absorption spectroscopy using tunable mid-infrared continuous-wave quantum cascade lasers. Appl Phys B 2011;102(2):417–23.

[25] Craig IM, Taubman MS, Lea AS, Phillips MC, Josberger EE, Raschke MB. Infrared near-field spectroscopy of trace explosives using an external cavity quantum cascade laser. Opt Express 2013;21(25):30401–14.

[26] Suter J, Bernacki B, Phillips M. Spectral and angular dependence of mid-infrared diffuse scattering from explosives residues for standoff detection using external cavity quantum cascade lasers. Appl Phys B 2012;108(4):965–74.

[27] Lee BH, Wood EC, Wormhoudt J, Shorter JH, Herndon SC, Zahniser MS, et al. Effective line strengths of trans-nitrous acid near $1275\ cm^{-1}$ and cis-nitrous acid at $1660\ cm^{-1}$. J Quant Spectrosc Radiat Transf 2012;113(15):1905–12.

[28] Rothman LS, Gordon IE, Barbe A, Benner DC, Bernath PE, Birk M, et al. The HITRAN 2008 molecular spectroscopic database. J Quant Spectrosc Radiat Transf 2009;110(9–10):533–72.

[29] Brown LR, Farmer CB, Rinsland CP, Toth RA. Molecular line parameters for the atmospheric trace molecule spectroscopy experiment. Appl Opt 1987;26(23):5154–82.

[30] Sironneau V, Flaud JM, Orphal J, Kleiner I, Chelin P. Absolute line intensities of HONO and DONO in the far-infrared and re-determination of the energy difference between the trans- and cis-species of nitrous acid. J Mol Spectrosc 2010;259(2):100–4.

[31] Chan WH, Nordstrom RJ, Calvert JG, Shaw JH. Kinetic study of HONO formation and decay reactions in gasous mixtures of HONO, NO, NO_2, H_2O, and N_2. Environ Sci Technol 1976;10(7):674–82.

[32] Robert HK, Arthur GM. Infrared absorption intensities of HONO. J Quant Spectrosc Radiat Transf 1983;30(1):37–44.

[33] Bongartz A, Kames J, Welter F, Schurath U. Near-UV absorption cross sections and trans/cis equilibrium of nitrous acid. J Phys Chem 1991;95(3):1076–82.

[34] Gratien A, Lefort M, Picquet-varrault B, Orphal J, Doussin JF, Flaud JM. Experimental intercomparison of the absorption cross-sections of nitrous acid (HONO) in the ultraviolet and mid-infrared spectral regions. J Quant Spectrosc Radiat Transf 2009;110(4–5):256–63.

[35] Yi H, Maamary R, Gao X, Sigrist MW, Fertein E, Chen W. Short-lived species detection of nitrous acid by external-cavity quantum cascade laser based quartz-enhanced photoacoustic absorption spectroscopy. Appl Phys Lett 2015;106(10). http://dx.doi.org/10.1063/1.4914896.

[36] Ferm M, Sjodin A. A sodium carbonate denuder determination of nitrous acid in the atmosphere. Atmos Environ 1985;19(6):979–83.

[37] Allegrini I, De SF, Di PV, Febo A, Perrino C, Possanzini M, et al. Annular denuder method for sampling reactive gases and aerosols in the atmosphere. Sci Total Environ 1987;67(1):1–16.

[38] Monge ME, D'Anna B, George C. Nitrogen dioxide removal and nitrous acid formation on titanium oxide surfaces – an air quality remediation process? Phys Chem Chem Phys 2010;12(31):8991–8.

[39] Febo A, Perrino C, Cortiello M. A denuder technique for the measurement of nitrous acid in urban atmospheres. Atmos Environ 1993;27A(11):1721–8.

[40] Acker K, Mfller D, Auel R, Wieprecht W, Kalag D. Concentrations of nitrous acid, nitric acid, nitrite and nitrate in the gas and aerosol phase at a site in the emission zone during ESCOMPTE 2001 experiment. Atmos Res 2005;74(1–4):507–24.

[41] Neftel A, Blatter A, Hesterberg R, Staffelbach T. Measurements of concentration gradients of HNO_2 and HNO_3 over a semi-natural ecosystem. Atmos Environ 1996;30(17):3017–25.

[42] Cui X, Lengignon C, Wu T, Zhao W, Wysocki G, Fertein E, et al. Photonic sensing of the atmosphere by absorption spectroscopy. J Quant Spectrosc Radiat Transf 2012;113(11):1300–16.

[43] Hancock G, Helden JH, Peverall R, Ritchie GAD, Walker RJ. Direct and wavelength modulation spectroscopy using a cw external cavity quantum cascade laser. Appl Phys Lett 2009;94(20):2011101–3.

[44] Zhao W, Gao X, Chen W, Zhang W, Huang T, Wu T, et al. Wavelength modulated off-axis integrated cavity output spectroscopy in the near infrared. Appl Phys B 2007;86(2):353–9.